HUBBLE IMAGING OF THE IONIZING RADIATION FROM A STAR-FORMING GALAXY AT $Z = 3.2$ WITH $f_{esc} > 50\%$[*]

E. VANZELLA[1], S. DE BARROS[1], K. VASEI[2], A. ALAVI[2], M. GIAVALISCO[3], B. SIANA[2], A. GRAZIAN[4], G. HASINGER[5], H. SUH[5],
N. CAPPELLUTI[6], F. VITO[7], R. AMORIN[4], I. BALESTRA[8,9], M. BRUSA[10,1], F. CALURA[1], M. CASTELLANO[4], A. COMASTRI[1],
A. FONTANA[4], R. GILLI[1], M. MIGNOLI[1], L. PENTERICCI[4], C. VIGNALI[10], AND G. ZAMORANI[1]

[1] INAF—Osservatorio Astronomico di Bologna, via Ranzani 1, I-40127 Bologna, Italy; eros.vanzella@oabo.inaf.it
[2] Departement of Physics and Astronomy, University of California, Riverside, CA 92507, USA
[3] Astronomy Department, University of Massachusetts, Amherst, MA 01003, USA
[4] INAF—Osservatorio Astronomico di Roma, via Frascati 33, I-00040 Monteporzio, Italy
[5] Institute for Astronomy, 2680 Woodlawn Drive, Honolulu, HI 96822, USA
[6] Yale Center for Astronomy and Astrophysics, Physics Department, New Haven, CT 06520, USA
[7] Department of Astronomy and Astrophysics, 525 Davey Laboratory, The Pennsylvania State University, University Park, PA 16802, USA
[8] INAF—Osservatorio Astronomico di Trieste, via G. B. Tiepolo 11, I-34131, Trieste, Italy
[9] University Observatory Munich, Scheinerstrasse 1, D-81679 München, Germany
[10] Dipartimento di Fisica e Astronomia, Universitá degli Studi di Bologna, Viale Berti Pichat 6/2, I-40127 Bologna, Italy

ABSTRACT

Star-forming galaxies are considered to be the leading candidate sources dominating cosmic reionization at $z > 7$: the search for analogs at moderate redshift showing Lyman continuum (LyC) leakage is currently an active line of research. We have observed a star-forming galaxy at $z = 3.2$ with *Hubble*/WFC3 in the F336W filter, corresponding to the 730–890 Å rest-frame, and detected LyC emission. This galaxy is very compact and also has a large Oxygen ratio [O III]$\lambda5007$/[O II]$\lambda3727$ ($\gtrsim 10$). No nuclear activity is revealed from optical/near-infrared spectroscopy and deep multi-band photometry (including the 6 Ms X-ray *Chandra* observations). The measured escape fraction of ionizing radiation spans the range 50%–100%, depending on the intergalactic medium (IGM) attenuation. The LyC emission is measured at $m_{F336W} = 27.57 \pm 0.11$ (with signal-to-noise ratio (S/N) = 10) and is spatially unresolved, with an effective radius of $R_e < 200$ pc. Predictions from photoionization and radiative transfer models are in line with the properties reported here, indicating that stellar winds and supernova explosions in a nucleated star-forming region can blow cavities generating density-bounded conditions compatible to optically thin media. Irrespective of the nature of the ionizing radiation, spectral signatures of these sources over the entire electromagnetic spectrum are of central importance for their identification during the epoch of reionization when the LyC is unobservable. Intriguingly, the *Spitzer*/IRAC photometric signature of intense rest-frame optical emissions ([O III]$\lambda\lambda4959,5007$ + Hβ) recently observed at $z \simeq 7.5$–8.5 is similar to what is observed in this galaxy. Only the *James Webb Space Telescope* will measure optical line ratios at $z > 7$, allowing a direct comparison with the lower-redshift LyC emitters, such as that reported here.

Key words: dark ages – first stars – galaxies: evolution – galaxies: high-redshift – reionization

1. INTRODUCTION

Cosmic reionization is a major episode in the history of the universe and the search for ionizing sources is one of the main goals of modern observational cosmology (Robertson et al. 2010). Star-forming galaxies and active galactic nuclei (AGNs) have been proposed to be the dominant sources of ionizing radiation, possibly active at different cosmic epochs (Haardt & Madau 2012). While the redshift evolution of the ultraviolet luminosity function of star-forming galaxies is relatively well measured up to $z \simeq 7$–8, showing that the bulk of the ultraviolet luminosity density is dominated by the faint galaxy population ($L < L^\star$, e.g., Bouwens et al. 2015), the number density of high-redshift and faint AGNs is still highly uncertain (e.g., Georgakakis et al. 2015; Giallongo et al. 2015). In addition, understanding the mechanisms of reionization (and post-reionization $z < 6$) hinges on assessing how the escape fraction of ionizing radiation, f_{esc} (LyC), changes as a function of luminosity

and redshift. Because of the intergalactic medium (IGM) opacity, direct observation of ionizing radiation during reionization is not feasible (Prochaska et al. 2010). A strategy to make progress is to identify LyC sources at lower redshift, e.g., $z \sim 3$–3.5, and study which of their observed properties can be used as predictors of an LyC leakage. Recent advances have been made by looking at starburst galaxies in the local universe (Borthakur et al. 2014; Izotov et al. 2016) at about 10 Gyr after reionization ended ($z \sim 6$). However, it is more useful to identify LyC leakers at the highest redshifts possible ($z \sim 3$, one billion years after the end of reionization) because these galaxies are likely better analogs to those that reionized the universe. For instance, LyC emitters identified in the nearby universe exhibit redder UV slopes than $z \sim 6$ galaxies (Borthakur et al. 2014; Izotov et al. 2016).

Escaping LyC radiation from galaxies has been searched in recent years (Siana et al. 2010; Vanzella et al. 2010b; Mostardi et al. 2013, 2015; Nestor et al. 2013) and, to date, no spectroscopically confirmed detection of LyC has been reported at high redshift (Siana et al. 2015). Moreover, nothing is known about the spatial distribution of the emerging LyC radiation. The difficulty of directly and unambiguously identifying LyC radiation in distant galaxies is due to a combination of several

effects: (1) superposition of foreground sources can produce false LyC detections (Vanzella et al. 2010b, 2012) and, in this respect, *Hubble Space Telescope* (*HST*) observations are crucial (Mostardi et al. 2015; Siana et al. 2015); (2) the intergalactic transmission in the ionizing domain is stochastic (Inoue et al. 2014); (3) the geometrical distribution of the neutral gas in galaxies and the relatively short duty cycle of f_{esc} (LyC) over cosmic time adds further stochasticity to the LyC visibility (Wise et al. 2014; Cen & Kimm 2015); (4) given the current sensitivity limits of large telescopes, it is only possible to probe an interesting dynamic range of LyC/non-ionizing UV ratios in galaxies with $L > 0.5L^\star$, a category for which the escape fraction of ionizing radiation has been shown to be intrinsically low ($<5\%$–10%, Vanzella et al. 2010a; Mostardi et al. 2015; Siana et al. 2015; Grazian et al. 2016). These aspects make the search for escaping ionizing radiation challenging and can explain the current low detection rate at high redshift. Nevertheless, the identification of examples with escaping LyC radiation lying in the tail of the large f_{esc} (LyC) values, though rare (Vanzella et al. 2010a), represents the only empirical method we have to increase our physical insight into the mechanisms that allow ionizing photons to escape, thus providing unique reference for studies at $z > 6$.

Here, we report on LyC emission arising from a distant galaxy ($z = 3.212$) unambiguously confirmed with *HST* observations. Throughout this paper, the AB magnitude system ($AB = 31.4 - 2.5 \log(f_\nu/nJy)$) and a cosmology of Ω_{tot}, Ω_M, $\Omega_\Lambda = 1.0, 0.3, 0.7$ with $H_0 = 70$ km s^{-1} Mpc^{-1} are used.

2. THE SELECTED CANDIDATE LyC EMITTER

An LyC candidate at $z = 3.212$ in the GOODS-Southern field, named *Ion2* (GDS-ID 033203.24-274518.8), was first identified by Vanzella et al. (2015). This candidate is a $\sim10^9 M_\odot$ galaxy with SFR $= 15.6 \pm 1.5 \, M_\odot$ yr^{-1} (sSFR ~ 10 Gyr^{-1}), EW(Lyα) $= 94 \pm 20$ Å, and EW([C III]$\lambda1909$) $= 18^{+9}_{-5}$ Å (de Barros et al. 2016). The compact star-forming region, showing strong [O III] $\lambda\lambda4959,5007$ emission lines (with a rest-frame equivalent width of 1500 Å) and a large Oxygen ratio [O III]$\lambda5007$/[O II]$\lambda3727$ ($\geqslant10$ at 1σ, de Barros et al. 2016) measured with Keck/MOSFIRE, makes *Ion2* the highest redshift "Green Pea" galaxy the currently known and, accordingly to the photoionization models (Jaskot & Oey 2013; Nakajima & Ouchi 2014), an ideal candidate LyC emitter. A plausible spectroscopic LyC detection was subsequently discussed in de Barros et al. (2016). However, the presence of a close companion not resolved with ground-based spectroscopy and imaging (0″2, see Figure 1) cast some doubts on the association of the observed flux with *Ion2*, and thus on the reliability of the LyC leakage. Thanks to the Lyβ and Lyγ detection in the Very Large Telescope (VLT)/VIMOS *Ion2* spectrum (see Figure 6 panel (A), or de Barros et al. 2016, Figure 2), the spectroscopic redshift of component A is unambiguously $z = 3.2$. The 4 hr exposure is not enough to detect such absorption features with a signal-to-noise ratio (S/N) of S/N > 5 (as observed here) for component B, which at these wavelengths is mag $= 27.2$ in the continuum.[11] Therefore these features arise from component A at $z = 3.2$. The [O III]
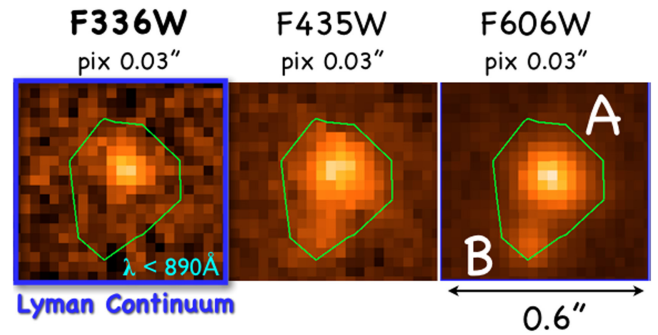

Figure 1. From left to right, the F336W, F435W, and F606W *HST*/ACS thumbnails of *Ion2*. LyC emission (rest-frame $\lambda < 890$ Å) arising from the brighter component (A) is evident in the F336W-band images. The green iso-contour derived from the F435W band guides the eye in comparing the shape of the source. Secondary emission (B), offset by 0″2, is visible below the main source in the F435W and F606W images, but not in the F336W image.
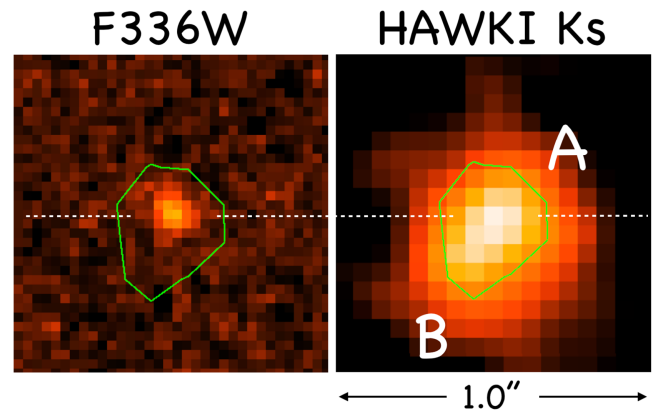

Figure 2. LyC *HST*/F336W (left) and VLT/HAWKI Ks-band (right) image thumbnails of *Ion2*. The dashed line marks the position of component A (see also Figure 1). The K-band emission is prominent from A, suggesting that the [O III]$\lambda\lambda4959,5007$ is arising mainly from component A.

emission is also mainly associated with component A because the K-band magnitude is dominated by the strong [O III] lines and the K-band spatial emission is more prominent from A. This is shown in Figure 2 where the VLT/HAWKI K-band image has been extracted from the HUGS survey (Fontana et al. 2014).

3. *HST* OBSERVATIONS

To confirm the LyC emission, we obtained *HST* WFC3/UVIS images in the F336W filter, which corresponds to rest-frame 730–890 Å. Seventeen 2800 s (1-orbit) dithered exposures were taken for a total integration time of 47.6 ks. The charge transfer efficiency (CTE) of the WFC3/UVIS CCDs has degraded significantly due to radiation damage and this was particularly problematic in images with low background. To mitigate the effects of poor CTE, we increased the background to $\sim12e^-$ pix^{-1} with a post-flash LED (Biretta & Baggett 2013). Furthermore, we placed the target near the read-out edge of the CCD so that the electron transfer occurred across only ~300 of the 2048 pixels. Finally, we applied a pixel-based CTE correction.[12] As the dark current was nearly half of the total background, proper dark subtraction was critical. Unfortunately, the STScI darks were only a single value and

---

[11] From ESO/Exposure Time Calculator, an S/N $\lesssim 1$ is expected at this magnitude, wavelength, and integration time. This would imply an S/N $\ll 1$ if Lyβ and Lyγ absorption lines arise from component B.

[12] http://www.stsci.edu/hst/wfc3/tools/cte_tools

did not allow us to capture the gradient and blotchy pattern in the dark current (Teplitz et al. 2013). Also, because the darks were not CTE-corrected, more than half of the hot and warm pixels were not properly masked (Rafelski et al. 2015). To mitigate these issues, we adopted the dark processing method explained in detail in Rafelski et al. (2015). First, we CTE-corrected all of the raw dark images in the anneal cycle of our visits and removed cosmic rays. We then found and masked the hot pixels that appeared throughout the anneal cycle and made a mean super dark from all of the darks in the anneal cycle. We then dark subtracted the science images while masking the hot pixels that were found to exist at the time of the observation.

We processed all of our CTE-corrected raw data using STSDAS task CALWF3, including subtraction of our new super darks. These calibrated images were then combined using Astrodrizzle (Gonzaga et al. 2012), which performs background subtraction, cosmic-ray rejection, and geometric distortion correction. The final combined F336W image had a pixel scale of 0.″03 and was astrometrically aligned with the three-dimensional-*HST* (3D-*HST*) F606W image (Skelton et al. 2014) with a precision of 48 mas. As a by-product, Astrodrizzle produced an inverse variance image that we used to derive the uncertainties in the photometry. We performed aperture photometry using a growth-curve methodology. The estimated uncertainty was corrected for the correlated noise introduced by the drizzling process (Casertano et al. 2000). Finally, we corrected our photometry for Galactic extinction (0.041 mag; Schlafly & Finkbeiner 2011).

4. RESULTS

The spectroscopic detection of the LyC emission reported by de Barros et al. (2016) is uncertain because of the presence of a secondary component (component B). If component B were at a lower redshift, then it could have contaminated the spectrum of the primary component, mimicking LyC emission. The *HST* imaging clearly solves the problem of the close neighbor by showing that the LyC emission arises only from component A (see Figure 1). The LyC emission is unambiguously confirmed at $S/N = 10$ with magnitude $m(F336W) = 27.57 \pm 0.11$. Also, for the first time, it provides spatial mapping of the ionizing radiation from a galaxy. From deep multi-wavelength observations, including *Chandra* 6 Ms image, *HST* optical (GOODS, Giavalisco et al. 2004) and near-infrared (CANDELS, Grogin et al. 2011), *Spitzer* (3.6, 4.5, 5.8, 8.0, 24 μm), and wide spectroscopic coverage from the U to K bands (VLT and Keck), we found *Ion2* to be a low-mass ($\leqslant 10^9 M_\odot$), low-metallicity ($\sim 1/6 Z_\odot$), star-forming galaxy (de Barros et al. 2016).

We derived the absolute escape fraction quantity, f_{esc} (LyC), with the usual formulation (e.g., Vanzella et al. 2012):

$$f_{esc}(\text{LyC}) = \frac{(L1500/L800)_{\text{INT}}}{(f1500/f800)_{\text{OBS}}}$$
$$\times \frac{1}{T(\text{IGM})_{F336W}} \times 10^{-0.4 \times A_{1500}}, \qquad (1)$$

which is related to the relative escape fraction, $f_{esc,rel}$ (LyC), as $f_{esc,rel}(\text{LyC}) = 10^{0.4 A_{1500}} f_{esc}(\text{LyC})$. Given the low dust attenuation derived in de Barros et al. (2016), $E(B - V) < 0.04$ ($A_{1500} < 0.4$), the relative and absolute fractions are very similar in this case (they coincide if $E(B - V) = 0$ or

$A_{1500} = 0$). For simplicity, we assume no dust attenuation. The $f1500/f800$ is the observed flux density ratio ($=14.60$) calculated on component A only (where the LyC arises) using the same circular apertures of 0.″2 radius and subtracting component B from the *HST*/ACS bands before running SExtractor on A, as described in Vanzella et al. (2015). T(IGM)$_{F336W}$ is the IGM transmission for the F336W filter, which is obtained by convolving the 10,000 IGM transmissions at $z = 3.2$ (Inoue et al. 2014) with the F336W transmission curve (as described in Vanzella et al. 2010a, 2015). The intrinsic luminosity density ratio $L1500/L800_{\text{INT}}$ is observationally uncertain and must be estimated from stellar population synthesis models.

Although we have a clear detection at ($\lambda < 890$ Å), it is not possible to compute a precise value of f_{esc} (LyC), which depends on the IGM transmission and the intrinsic luminosity density ratio, $L1500/L800_{\text{INT}}$. Therefore we derive a range of plausible values taking advantage of the detected LyC signal ($m(F336W) = 27.57 \pm 0.11$). A range of possible IGM transmissions is obtained by assuming that the minimum theoretical intrinsic flux density ratio is 1 (e.g., Siana et al. 2007) and that f_{esc} (LyC) $\leqslant 1$ (Vanzella et al. 2012). Under these assumptions, the IGM transmission T(IGM)$_{F336W}$ cannot be lower than 0.068 (otherwise m(F336W) would be brighter than the magnitude at 1500 Å). In Figure 3, we show the resulting f_{esc} (LyC) distribution adopting T(IGM)$_{F336W} > 0.068$ and the intrinsic ratio ($L1500/L800)_{\text{INT}} = 5$. The latter is an intermediate value between the predictions for an instantaneous burst and the predictions for a constant star formation history (Siana et al. 2007): given the ionizing photon production rate (see next section) and the age derived from SED fitting (de Barros et al. 2016), we expect the intrinsic ratio to be between ~ 3 and ~ 7. In particular, the observed LyC emission suggest the presence of O-type stars, and consequently an interval of time since the onset of the last burst of a few million years.

In the most extreme case, adopting ($L1500/L800)_{\text{INT}} > 1$ and the maximum IGM transmission, the minimum f_{esc} (LyC) is 10%. However, as shown in Figure 3, the degeneracy introduced by the IGM stochasticity prevents us from placing strong constraints on f_{esc} (LyC) or ($L1500/L800)_{\text{INT}}$, as various combinations of f_{esc} (LyC), ($L1500/L800)_{\text{INT}}$, and T(IGM) can produce the observed F336W flux. Adopting ($L1500/L800)_{\text{INT}} = 5$, an f_{esc} (LyC) of 50(100)% is derived if T(IGM)$_{F336W}$ is 34(73)%. It is worth noting that this source has been selected as a candidate LyC emitter with a method that eventually favors IGM and/or ISM transparencies (Vanzella et al. 2015). Therefore, an IGM transmission higher than the average along this line of sight would be not surprising.

4.1. The Ionizing Photon Production Rate

The measured ionizing photon production rate corresponding to the observed m(F336W) $= 27.57$ is $N_{phot}(800$ Å) $= 1.7 \times 10^{53}$ s^{-1}. The statistical error related to the measured magnitude is negligible when compared to the stochasticity of the IGM attenuation affecting a single line of sight, as shown by the distribution of F336W–IGM convolved transmissions derived from the IGM prescription of Inoue et al. (2014; T(IGM)$_{F336W}$, Figure 3). Assuming the maximum T(IGM)$_{F336W}$ allowed at $z = 3.2$ ($\simeq 70\%$), we have an intrinsic m(F336W) $= 27.18$ that corresponds to

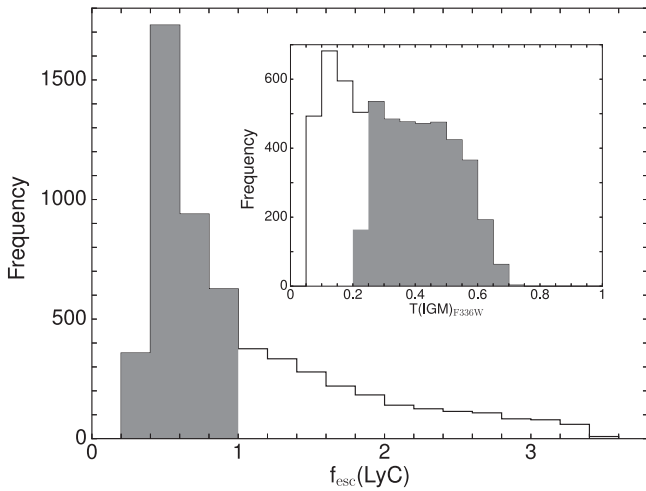**Figure 4.** Difference between the observed F336W image (A) GALFIT best-fit model calculated in the F435W image (B) is shown in the right (A–B). Model A is scaled to the flux peak of the F336W source (B). This comparison suggests that the LyC emitting region is more compact than the resolved emission measured in the F435W band. In the right panel, the residuals after subtracting a star rescaled to the source flux are shown. The size of the thumbnails is $1''2 \times 1''0$.

Figure 3. Distribution of f_{esc} (LyC) is shown in the main panel adopting an intrinsic luminosity density ratio $(L1500/L800)_{INT} = 5$ (see Equation (1)). We adopt a minimum ratio of $(L1500/L800)_{INT} = 1$ and f_{esc} (LyC) $\leqslant 1$ to exclude unphysical IGM transmissions $(T(IGM)_{F336W} > 0.068)$. Values of f_{esc} (LyC) > 3.5 have been fixed to 3.5 to better display the entire distribution. f_{esc} (LyC) $\leqslant 1$ corresponds to 63% of the realizations (gray histogram). The inset shows the IGM transmission at $z = 3.2$ (from Inoue et al. 2014), excluding unphysical IGM transmission values and showing in gray those consistent with f_{esc} (LyC) $\leqslant 1$.

N_{phot} (800 Å) $= 2.5 \times 10^{53}$ s^{-1}. We can set a conservative upper limit to N_{phot} by assuming that the intrinsic F336W magnitude (ionizing emission) cannot be brighter than the observed magnitude at 1500 Å rest-frame ($\sim$24.66), i.e., the intrinsic luminosity density ratio is $L1500/L800 > 1$ (i.e., no extreme stellar populations are present). We obtain N_{phot} (800 Å) $= 2.5 \times 10^{54}$ s^{-1}. Therefore, the intrinsic ionizing photon production rate is 2.5×10^{53}s$^{-1} \leqslant N_{phot}$ (800 Å) $\leqslant 2.5 \times 10^{54}$ s^{-1}. We discuss the implications of this value in Section 5.2.

4.2. LyC Morphology

The LyC leakage is co-spatial with component A and nothing is detected from component B, where A and B refer to the brighter and the fainter blobs, respectively (see Figure 1, following the Vanzella et al. 2015 nomenclature). *Ion2* is a compact but well-resolved galaxy in the F435W, F606W, F775W, and F850LP ACS images, corresponding to the rest-frame far-UV from 1030 to 2020 Å. The galaxy, however, does not appear to be resolved in the WFC3 F336W image. We took a well-exposed, nearby bright star and inserted it into a blank area of the image at random positions to simulate a number ($N = 50$) of realizations of the point-spread function (PSF), after rescaling it to the same flux as *Ion2*. We then aligned the star at the same position of the light centroid of *Ion2* and subtracted it, in each case obtaining residuals consistent with the sky background (an example is shown in Figure 4). We have also compared the morphology of *Ion2* in the F336W and F435W bands to test the possibility that the lower S/N in the former band is the reason for the apparent unresolved morphology, adopting the following procedure. Basic PSF-corrected morphological information from both components was extracted by Vanzella et al. (2015) using GALFIT (Peng et al. 2010). Given their regular (symmetric) morphology, the GALFIT modeling with a Gaussian light profile well reproduces both regions in all of th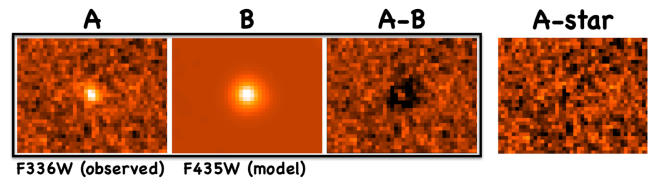e ACS images and shows that they are spatially resolved with effective radii of a few hundred parsecs. In particular, in Figure 5, we show the result obtained at 1000 Å rest-frame (F435W band) adopting a Gaussian shape. The best solution produces an effective radius of $R_e = 340 \pm 25$ pc, suggesting that the stellar radiation emerges from a compact and resolved region; the error has been calculated by running GALFIT on simulated images obtained by inserting the B-band model into random and free regions of the F435W-band image. GALFIT fitting on the LyC image does not produce resolved solutions. In order to characterize the LyC morphology, we perform a simple test by subtracting the best-fit B435-band model from the F336W image. After normalizing the two images at the same flux peak and checking the residuals over a grid of dimming factors, it turns out that the LyC emission arises from a region smaller than what has been inferred from the F435W-band observations (see Figure 4); in particular, the spatially unresolved image in F336W has an effective radius <200 pc. The negative residual flux seen in Figure 4 extends at least to 5 pixels radially from the center, and cannot be explained by the small variations in the PSFs at the two wavelengths. The observed compactness of the LyC emission is probably not surprising if we compare our *HST* resolution to the size of the super-star clusters observed in local starbursts, in which the O-type stars are spatially segregated toward the center within tens of parsecs (e.g., Annibali et al. 2015; James et al. 2016).

Another possible interpretation is that the LyC emission of *Ion2* could originate from an AGN. This is unlikely and is discussed in Section 5.1.

5. DISCUSSION

Independent of the nature of ionizing photons, the LyC detection implies a low column density of neutral gas along the line of sight, lower than $10^{17.2}$ cm^{-2} (corresponding to τ (LyC) < 1). de Barros et al. (2016) have shown for the first time empirical evidence linking high f_{esc} (LyC) with the compactness of the star-forming region, the large [O III]/[O II] line ratio, the weak ultraviolet interstellar absorption lines, and the emerging Lyα emission close to the systemic redshift, as predicted by photoionization and radiative transfer models when the medium is considered to be optically thin (Jaskot & Oey 2013; Borthakur et al. 2014; Nakajima & Ouchi 2014; Verhamme et al. 2015; Izotov et al. 2016). The *HST* observations presented here unambiguously confirm those predictions.
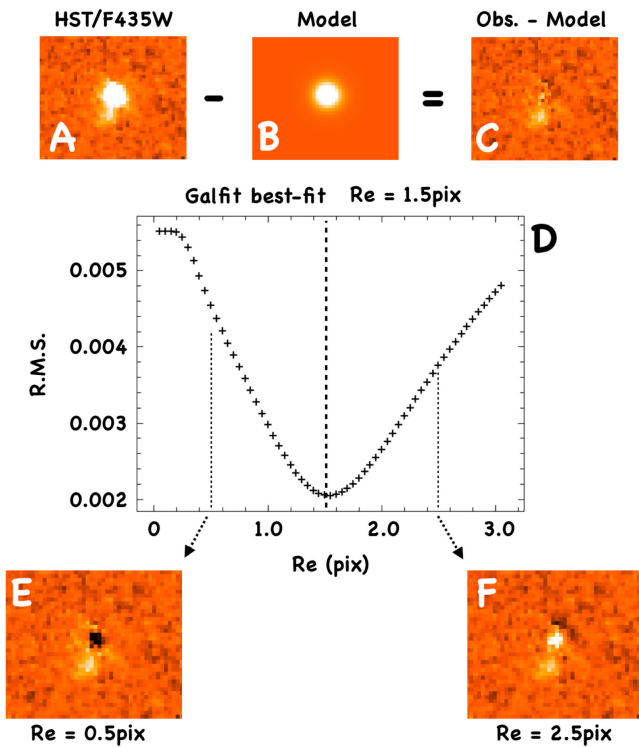
Figure 5. GALFIT modeling of the *Ion2* galaxy in the F435W band (1000 Å rest-frame). In panel (C), the residuals of the observed (A)-model (B) are shown for the best-fit case ($R_e = 1.5$ px $\simeq 340$ pc). Bottom panels show an example of two "bad" solutions (observed-model), in which positive/negative residuals are evident (panels (E)/(F)). Middle panel (D) shows the behavior of the rms calculated at the "A" position by running GALFIT in a grid of effective radii (as described in Vanzella et al. 2015). A good convergence is reached at $R_e = 1.5 \pm 0.1$ px. This illustrates that the source is spatially resolved at 1000 Å rest-frame. The size of the thumbnails is $1''.2 \times 1''.0$.

5.1. Nature of the Source of the LyC Photons

In the following, we summarize a few key elements (de Barros et al. 2016) and add new empirical and theoretical evidence that favors the stellar origin of the ultraviolet light rather than an AGN origin.

1. No high-ionization emission lines like N vλ1240, C IVλ1550, or He IIλ1640 have been detected at more than the 3σ level from the VLT/VIMOS MR spectrum (Figure 6), while the [CIII]λ1909 line is clearly detected. From the C IVλ1550/[C III]λ1909 < 0.15 and [C III]λ1909/He IIλ1640 > 4.0 line ratios, and following Feltre et al. (2016), this source is classified as a star-forming galaxy lying in the same region occupied by low-metallicity galaxies of Stark et al. (2014).

2. *Ion2* is spatially resolved in all of the ACS bands (340 ± 25 pc) implying that the stellar emission is dominating the observed range 1000–2000 Å rest-frame.

3. The narrow width of the [O III]λ5007 emission line ($\sigma = 65$ km s^{-1}) is compatible with lower-redshift star-forming galaxies (Maseda et al. 2014), while the AGN population typically shows higher velocity dispersions (>200 km s^{-1}, e.g., Osterbrock & Mathews 1986).

4. *Ion2* is not detected in the X-ray in the 4 Ms CDFS (Cappelluti et al. 2016) and no evidence of emission is inferred from the recent *Chandra* pointings publicly

available on the *Chandra* website[13], which increased the exposure time to ∼6 Ms (see Figure 6). This places a limit on the X-ray luminosity of $L_X \lesssim 3 \times 10^{42}$ erg s^{-1} at the 1σ limit. If *Ion2* were a type I AGN, and assuming that the L_X–$L_{[OIII]}$ relation observed locally is valid at $z = 3$, then the measured [O III]λ5007 luminosity (de Barros et al. 2016) would imply a detection with S/N > 100 at the *Ion2* position in the 6 Ms X-ray image, corresponding to $L_X \simeq 10^{45}$ erg s^{-1} (Panessa et al. 2006; Ueda et al. 2015). The measured [O III]λ5007 line luminosity (2×10^{43} erg s^{-1}) and the non-detection in the 6 Ms X-ray would imply a high obscuration (if it were an AGN), formally with an equivalent column density $N_H > 10^{25}$cm^{-2} (assuming solar metallicity). The estimated stellar mass from the LyC source is ∼$10^8 M_\odot$ (see Section 5.2) and, following Maseda et al. (2014), the dynamical mass from the [O III]λ5007 line width ($\sigma = 65$ km s^{-1}) is ∼$10^9 M_\odot$. A lower limit on the BH mass of $10^8 M_\odot$ can be estimated by converting the [O III] λ5007 line luminosity into an AGN bolometric luminosity (Panessa et al. 2006; Lusso et al. 2012) and then assuming that the AGN is radiating at the Eddington limit. This mass would imply a very unusual and probably unrealistic ratio of $M_{\rm BH}$/Total mass $\geqslant 0.1$ for this object.

5. Adopting the expected L_X (from [O III]λ5007 reported above), we expect a clear detection at 6 μm rest-frame (i.e., at 24 μm observed with *Spitzer*/MIPS) by assuming that the relation between L_X and L (6 μm) (Stern 2015) is valid. In particular, even when adopting an $L_X > 10^{44}$ erg s^{-1}, we expect $L(6\ \mu m) > 10^{44}$ erg s^{-1} that corresponds to mag (24 μm) < 20(AB) and therefore a detection in the MIPS 24 μm image at S/N > 10. At the position of *Ion2*, no signal is detected in the MIPS 24 μm band down to AB $\simeq 22.3$ (de Barros et al. 2016).

It is worth noting a photometric excess (S/N > 5) in the second IRAC channel at 4.5 μm (Figure 6) that we ascribed to possible He Iλ10830+Pγ lines with rest-frame equivalent width of ∼1100 Å. While these lines can only be observed with the *James Webb Space Telescope* (*JWST*), such strong He Iλ10830 emission up to a 1000 Å equivalent width has been observed in local compact H II regions by Izotov et al. (2014) and in a local LyC emitter candidate (Verhamme et al. 2015).

Therefore, we conclude that the signal observed in the *HST*/F336W band is very likely due to stellar emission; the only (unlikely) alternative would be the presence of a heavily obscured AGN, located at the center of the star-forming region and hidden by gas and dust at all wavelengths but visible in the ionizing continuum, a possibility we deem very contrived. An intrinsically faint AGN could co-exist with dominant star formation activity that controls the transparency of the medium. In this regard, we already proposed in Vanzella et al. (2015) the possible hybrid configuration in which stellar and non-stellar (AGN) ionizing emission could co-exist in some systems and might explain the tension found between the UV excess and the stellar population synthesis models reported in the literature. In the present case, a partial AGN contribution could also explain the LyC leakage, although a more dedicated discussion of the physical mechanisms that lower the column density of neutral gas would be needed and this is beyond the scope of this work.
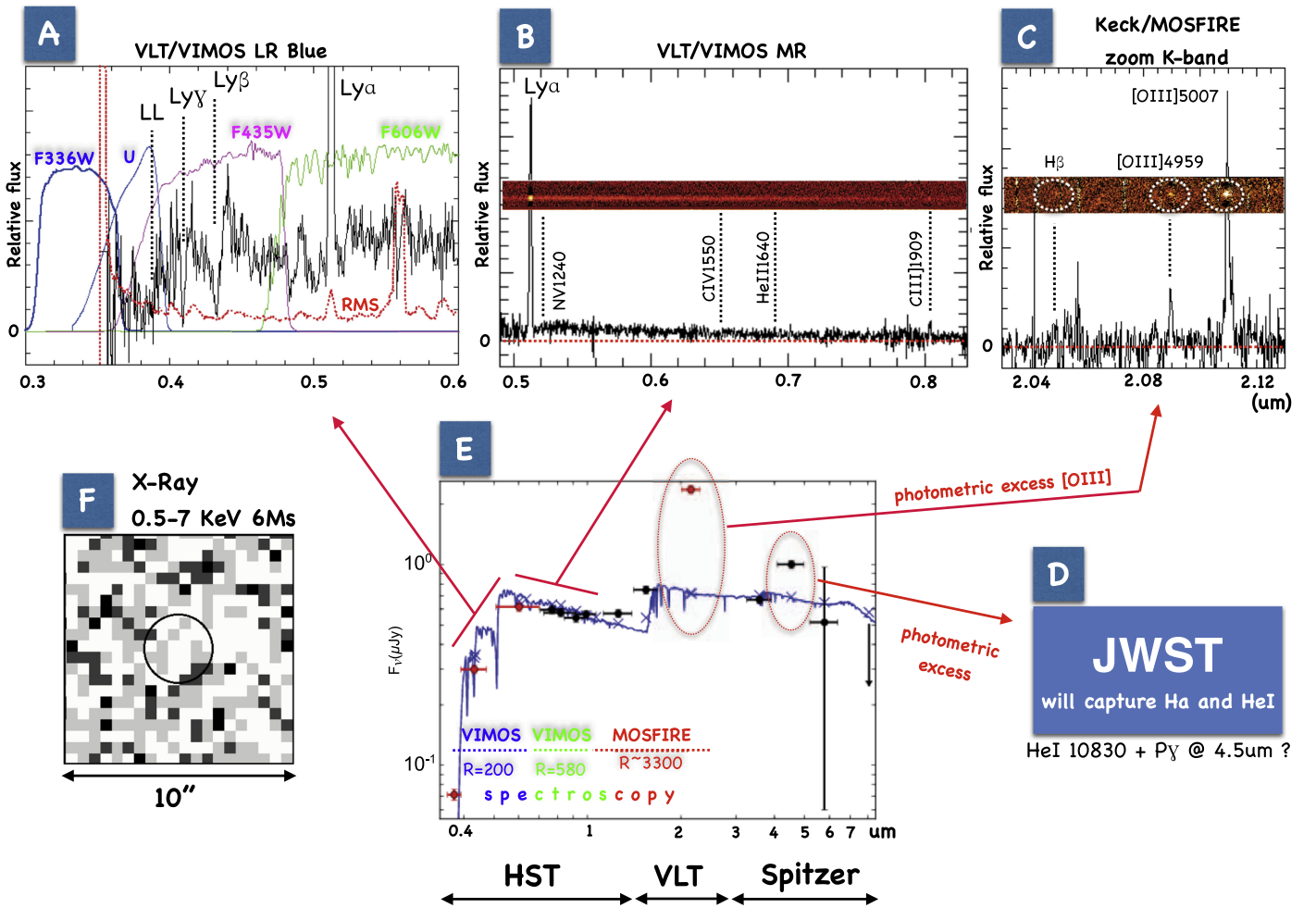
---

[13] http://cxc.harvard.edu/

Figure 6. Panoramic view of the available multi-frequency data for *Ion2* from the 0.35 to 2.4 μm wavelength range (VLT/VIMOS and Keck/MOSFIRE). Panels (A), (B), and (C): spectral coverage from the U to K bands with VLT/VIMOS and Keck/MOSFIRE. The insets of panels (B) and (C) show the two-dimensional spectra. The absence of high-ionization emission lines (N Vλ1240, C IVλ1550, He IIλ1640) is evident, as is the clear detection of the Lyα and [C III]λ1909 lines. The [O III] $\lambda\lambda$4959,5007 lines from the Keck/MOSFIRE spectrum are also shown (from de Barros et al. 2016). In panel (E), a schematic view of the spectral SED fitting indicating the available observations (VLT, Keck, *HST*, *Spitzer*) is shown. *JWST* can cover the part at 2.4–5 μm, including lines as Hα and He Iλ10830, not accessible with current instruments (panel (D)). Panel (F) shows the 6 Ms X-ray 0.5–7 keV *Chandra* cutout (10″ × 10″) around *Ion2* obtained from the public *Chandra* observation (the circle of diameter 3″ marks the position of *Ion2*). The source is off-axis, and thus the PSF of the source would cover the entire circle symbol.

Moreover, despite the excellent deep multi-wavelength coverage, dedicated observations will be necessary to detect a possible faint AGN. For example, monitoring for variability could be a powerful diagnostic. Currently, there is no observational evidence of nuclear activity in this object, while stellar emission is certainly detected in all of the *HST* images.

5.2. Constraining the Burst of Star Formation

The measured ionizing photon production rate and the comparison with Starburst99 models (Leitherer et al. 1999) adopting an instantaneous burst, $Z = 0.004$, and a Salpeter IMF provide a stellar mass involved in the starburst event in the range 5×10^6–5×10^7 $M_\odot$ (depending on the intergalactic medium (IGM) transmission), with the young stellar component (<10 Myr) dominating the ionizing radiation in which the number of O-type stars ranges between 2×10^4 and 2×10^5. The ionizing photon production rate is similar to that derived at lower redshift for a recently discovered LyC emitter (Izotov et al. 2016).

Such a young starburst event can generate substantial ionizing radiation and produce ionized cavities, and recent supernovae and stellar winds may have carved holes (e.g., Weaver et al. 1977; Calura et al. 2015) in the ISM that favor LyC photon escape into the intergalactic medium. It is worth stressing that the observed large [O III]/[O II] line ratio (>10) is expected in this scenario (Jaskot & Oey 2013; Nakajima & Ouchi 2014). Similar large [O III]/[O II] ratios have been observed in local starbursts (James et al. 2016) in which the younger stellar component containing O-type stars is identified in the core of the starburst (similarly to what is inferred here) and can photoionize regions out to hundreds of parsecs, as has also been observed in a local starburst by Annibali et al. (2015). It is worth noting that the differential depression of nebular emission between Balmer and metal lines when a substantial leakage of ionizing radiation is present could strongly affect the usual diagnostic diagrams that separate star-forming versus AGN emission (e.g., BPT, Baldwin et al. 1981); in particular, an LyC emitter would move toward the AGN cloud if the Balmer lines were attenuated first.

6. CONCLUSIONS

While the LyC emitter reported here is rare among sources with similar luminosity (Vanzella et al. 2010a; Grazian et al. 2016), the non-ionizing multi-frequency properties observed in our galaxy and the confirmed LyC emission provide valuable prospects for the characterization of similar or fainter sources in the higher-redshift domain. In particular, the confirmed $z > 7.5$ galaxies (Finkelstein et al. 2013; Oesch et al. 2015; Zitrin et al. 2015) show particularly strong Oxygen and Balmer structure ([O III]$\lambda\lambda$4959,5007 + Hβ), at the same level as reported here (equivalent widths larger than 800–1000 Å rest-frame). It is premature to conclude that those sources effectively have an $f_{\rm esc}$ (LyC) > 0, as optical line ratios are needed to perform a direct comparison and this must be postponed until *JWST* launch. Our result is currently a unique high-redshift reference, both in terms of large Oxygen line ratio and large line equivalent width, and needs to be extended to statistically significant samples, especially investigating the faint luminosity domain. However, it demonstrates the feasibility of the identification of ionizing sources during the reionization epoch.

REFERENCES

Annibali, F., Tosi, M., Pasquali, A., et al. 2015, arXiv:1505.05545
Baldwin, J. A., Phillips, M. M., & Terlevich, R. 1981, PASP, 93, 5
Biretta, J., & Baggett, S. 2013, WFC3 Post-Flash Calibration, Tech. rep.
Borthakur, S., Heckman, T. M., Leitherer, C., & Overzier, R. A. 2014, Sci, 346, 216
Bouwens, R. J., Illingworth, G. D., Oesch, P. A., et al. 2015, ApJ, 811, 140
Calura, F., Few, C. G., Romano, D., & D'Ercole, A. 2015, ApJL, 814, L14
Cappelluti, N., Comastri, A., Fontana, A., et al. 2016, ApJ, 823, 95
Casertano, S., de Mello, D., Dickinson, M., et al. 2000, AJ, 120, 2747
Cen, R., & Kimm, T. 2015, ApJL, 801, L25
de Barros, S., Vanzella, E., Amorín, R., et al. 2016, A&A, 585, A51

Feltre, A., Charlot, S., & Gutkin, J. 2016, MNRAS, 456, 3354
Finkelstein, S. L., Papovich, C., Dickinson, M., et al. 2013, Natur, 502, 524
Fontana, A., Dunlop, J. S., Paris, D., et al. 2014, A&A, 570, A11
Georgakakis, A., Aird, J., Buchner, J., et al. 2015, MNRAS, 453, 1946
Giallongo, E., Grazian, A., Fiore, F., et al. 2015, A&A, 578, A83
Giavalisco, M., Ferguson, H. C., Koekemoer, A. M., et al. 2004, ApJL, 600, L93
Gonzaga, S., et al. 2012, The DrizzlePac Handbook
Grazian, A., Giallongo, E., Gerbasi, R., et al. 2016, A&A, 585, A48
Grogin, N. A., Kocevski, D. D., Faber, S. M., et al. 2011, ApJS, 197, 35
Haardt, F., & Madau, P. 2012, ApJ, 746, 12
Inoue, A. K., Shimizu, I., Iwata, I., & Tanaka, M. 2014, MNRAS, 442, 1805
Izotov, Y. I., Orlitová, I., Schaerer, D., et al. 2016, Natur, 529, 159160
Izotov, Y. I., Thuan, T. X., & Guseva, N. G. 2014, MNRAS, 445, 778
James, B. L., Auger, M., Aloisi, A., Calzetti, D., & Kewley, L. 2016, ApJ, 816, 40
Jaskot, A. E., & Oey, M. S. 2013, ApJ, 766, 91
Leitherer, C., Schaerer, D., Goldader, J. D., et al. 1999, ApJS, 123, 3
Lusso, E., Comastri, A., Simmons, B. D., et al. 2012, MNRAS, 425, 623
Maseda, M. V., van der Wel, A., Rix, H.-W., et al. 2014, ApJ, 791, 17
Mostardi, R. E., Shapley, A. E., Nestor, D. B., et al. 2013, ApJ, 779, 65
Mostardi, R. E., Shapley, A. E., Steidel, C. C., et al. 2015, ApJ, 810, 107
Nakajima, K., & Ouchi, M. 2014, MNRAS, 442, 900
Nestor, D. B., Shapley, A. E., Kornei, K. A., Steidel, C. C., & Siana, B. 2013, ApJ, 765, 47
Oesch, P. A., van Dokkum, P. G., Illingworth, G. D., et al. 2015, ApJL, 804, L30
Osterbrock, D. E., & Mathews, W. G. 1986, ARA&A, 24, 171
Panessa, F., Bassani, L., Cappi, M., et al. 2006, A&A, 455, 173
Peng, C. Y., Ho, L. C., Impey, C. D., & Rix, H.-W. 2010, AJ, 139, 2097
Prochaska, J. X., O'Meara, J. M., & Worseck, G. 2010, ApJ, 718, 392
Rafelski, M., Teplitz, H. I., Gardner, J. P., et al. 2015, AJ, 150, 31
Robertson, B. E., Ellis, R. S., Dunlop, J. S., McLure, R. J., & Stark, D. P. 2010, Natur, 468, 49
Schlafly, E. F., & Finkbeiner, D. P. 2011, ApJ, 737, 103
Siana, B., Shapley, A. E., Kulas, K. R., et al. 2015, ApJ, 804, 17
Siana, B., Teplitz, H., Colbert, J., et al. 2007, ApJ, 668, 62
Siana, B., Teplitz, H. I., Ferguson, H. C., et al. 2010, ApJ, 723, 241
Skelton, R. E., Whitaker, K. E., Momcheva, I. G., et al. 2014, ApJS, 214, 24
Stark, D. P., Richard, J., Siana, B., et al. 2014, MNRAS, 445, 3200
Stern, D. 2015, ApJ, 807, 129
Teplitz, H. I., Rafelski, M., Kurczynski, P., et al. 2013, AJ, 146, 159
Ueda, Y., Hashimoto, Y., Ichikawa, K., et al. 2015, ApJ, 815, 1
Vanzella, E., de Barros, S., Castellano, M., et al. 2015, A&A, 576, A116
Vanzella, E., Giavalisco, M., Inoue, A. K., et al. 2010a, ApJ, 725, 1011
Vanzella, E., Guo, Y., Giavalisco, M., et al. 2012, ApJ, 751, 70
Vanzella, E., Siana, B., Cristiani, S., & Nonino, M. 2010b, MNRAS, 404, 1672
Verhamme, A., Orlitová, I., Schaerer, D., & Hayes, M. 2015, A&A, 578, A7
Weaver, R., McCray, R., Castor, J., Shapiro, P., & Moore, R. 1977, ApJ, 218, 377
Wise, J. H., Demchenko, V. G., Halicek, M. T., et al. 2014, MNRAS, 442, 2560
Zitrin, A., Labbé, I., Belli, S., et al. 2015, ApJL, 810, L12